Active Steering in Small-Scale Soft Growing Robots for Enhanced Loop Closure Grasping

by

Drake H. Elliott

Submitted to the Department of Mechanical Engineering
in partial fulfillment of the requirements for the degree of

BACHELOR OF SCIENCE IN MECHANICAL ENGINEERING

at the

MASSACHUSETTS INSTITUTE OF TECHNOLOGY

May 2026

© 2026 Drake H. Elliott. This work is licensed under a CC BY-NC-SA 4.0 license.

The author hereby grants to MIT a nonexclusive, worldwide, irrevocable, royalty-free license to exercise any and all rights under copyright, including to reproduce, preserve, distribute and publicly display copies of the thesis, or release the thesis under an open-access license.

Authored by: Drake H. Elliott
Department of Mechanical Engineering
May 8, 2026

Certified by: Harry Asada
Professor of Mechanical Engineering, Thesis Supervisor

Accepted by: Daniel Frey
Professor of Mechanical Engineering
Undergraduate Officer

Active Steering in Small-Scale Soft Growing Robots for Enhanced Loop Closure Grasping

by

Drake H. Elliott

Submitted to the Department of Mechanical Engineering
on May 8, 2026 in partial fulfillment of the requirements for the degree of

BACHELOR OF SCIENCE IN MECHANICAL ENGINEERING

ABSTRACT

This thesis proposes the development and integration of active steering articulation into small-scale soft growing robots (i.e., "vine robots") to enhance loop closure grasping. The manipulation of objects that are simultaneously heavy and fragile represents a persistent challenge in robotics. Traditional rigid grippers rely on high, localized compressive forces, while highly compliant soft grippers inherently lack the structural rigidity required to bear substantial payloads. Loop closure grasping transforms a grasping mechanism's topology from an open to a closed loop, overcoming traditional single-morphology trade-offs to achieve simultaneously strong, gentle, and versatile grasps [1]. Currently, these systems use soft-growing robots because their initial open-loop topology enables navigation through complex, highly constrained environments without sliding friction. Once the tip is fastened to the base, the deflated closed-loop structure leverages high tensile strength and infinite bending compliance to safely cradle objects. While current implementations rely on pre-forming to mechanically program the initial growth trajectory, the lack of active articulation limits the system's ability to reliably navigate the robot's tip into the fastening mechanism.

This thesis details the design and fabrication of pneumatic artificial muscles constructed from low-density polyethylene membranes integrated onto pre-formed vine robots for loop closure grasping. These actuators superimpose continuous active curvature over discrete pre-programmed bends. We develop and empirically validate a kinematic superposition model to accurately predict the pneumatic manipulator's bending curvatures under varying actuation pressures and pre-formed bend parameters. A physical prototype and experimental results demonstrate successful active loop closure, wherein the actuators correct trajectory deviations to guide the tip into passive anchoring clamps. Experimental validation confirms that the proposed system safely lifts 6.3 kg with an assembly mass of only 1.4 kg. The system exceeded quantitative targets for maximum local curvature (4.74°/cm) and total bending angle (229.4°), confirming the kinematic and load-bearing advantages of the actively steered closed-loop design.

Thesis supervisor: Harry Asada
Title: Professor of Mechanical Engineering

Acknowledgments

I would like to thank my thesis supervisor, Professor Harry Asada, for the opportunity to conduct this research within the d'Arbeloff Laboratory. I am also grateful to Kentaro Barhydt for his direct mentorship and insight throughout the process. Finally, I thank Andrew Pignataro for his assistance with the physical fabrication and experimental validation of this system.

Contents

List of Figures

List of Tables

Chapter 1

Introduction

The safe and secure manipulation of objects that are both heavy and fragile is a profound challenge in robotics. Conventional rigid grippers rely on localized compressive forces, which excel at precise positioning and bearing high payloads but are unsuitable for delicate targets due to the risk of failure [1]. Conversely, highly compliant soft grippers distribute forces gently but lack the structural rigidity to lift dense, heavy objects [1].

Tip-everting soft growing robots, or "vine robots," however, have shown significant promise for bearing heavy loads by utilizing the passive tensile strength of their membrane material [2]. Due to their thin-walled construction, they can act as highly compliant slings when deflated. Furthermore, they are highly effective at navigating around objects and into desired configurations because their extension bypasses sliding friction, allowing them to traverse tightly constrained environments [3]. These properties make vine robots a highly promising mechanism for loop closure grasping. Loop closure grasping works by decoupling grasp creation and grasp holding through a dynamic topological transformation [1]. The grasping mechanism begins with an open-loop topology to navigate the environment and encircle the object. Once the tip reaches the base frame, it is mechanically fastened, transitioning into a closed-loop structure [1]. The deflated, high-tensile membrane provides a cradle-like grasp with infinite bending compliance, distributing forces safely across the target [1].

However, small-scale implementations currently rely on passive pre-forming, mechanically programming permanent discrete bends into the robot body [4]. Pre-forming lacks the articulation necessary to dynamically correct the robot's path if it encounters unpredicted environmental disturbances or if there are manufacturing errors in the pre-forming. This thesis aims to address this gap by designing, fabricating, and validating an active steering articulation system integrated with pre-formed vine robots. Superimposing actuators onto a pre-form provides a unique and highly beneficial solution for loop closure grasping. Traditional active steering mechanisms are designed to maintain the freedom to bend in any direction. In loop closure grasping, however, the approximate trajectory required to encircle the object is already known. This allows us to intentionally bias the bending direction with a pre-form, establishing both robust navigation and a tight baseline curve. The core contributions of the thesis are: (1) the mechanical design and kinematic modeling of a pre-formed vine robot articulated by pouch motors for loop closure grasping, (2) a physical prototype integrating these appendages into a complete multi-base gripper mechanism, and (3) the experimental validation of the system and demonstration of active loop closure grasping.

Chapter 2

Related Work

The foundational mechanics of soft growing robots were established by Hawkes et al., who demonstrated that an inverted thin-walled vessel can navigate highly constrained spaces via pressure-driven eversion [3]. Blumenschein et al. reviewed the modeling, design, and control of vine robots, highlighting the need for specialized steering mechanisms as quasi-static growth models alone cannot account for spatial articulation [5].

To control the trajectory of vine robots, several actuation methods have been explored. Passive steering via pre-forming reliably dictates fixed growth paths by taping or welding discrete folds into the robot's body [4]. Active steering is typically achieved using distributed strain actuators. Kübler et al. compared three pneumatic actuators for vine robots: the pouch motor, the Cylindrical Pneumatic Artificial Muscle (cPAM), and the Fabric Pneumatic Artificial Muscle (fPAM) [6]. While cPAMs yield the highest lateral forces and fPAMs actuate the fastest, pouch motors offer the simplest manufacturing process for small-scale disposable systems [6]. Furthermore, finite element analysis (FEA) by du Pasquier et al. validated that geometry-based contraction from these actuators accurately generates significant, distributed buckling deformations [7].

In the context of soft grasping, alternative approaches like stochastic topological grasping utilize arrays of active elastomer filaments to entangle geometrically complex objects [8]. Similarly, dynamic weaving of entangled closed loops has been shown to produce exceptionally high payload-to-weight ratios (up to 770) [9]. However, these entanglement strategies require objects to be within the immediate operational radius and cannot navigate deep clutter. Moreover, these methods cannot dynamically transition from open to closed-loop topologies, or vice versa.

The loop closure grasping framework resolves this by utilizing vine robots to decouple the spatial navigation phase from the high-tensile load-bearing phase [1]. This research builds directly on these findings by introducing an actively steered hybrid method that guarantees the robot tip correctly threads into the anchoring mechanism, ensuring robust loop closure even without favorable environmental contact.

Chapter 3

System Requirements

The design, fabrication, and validation of the active steering articulation system are governed by a strict set of quantitative targets, optimizing the system for small-scale deployment, high maneuverability, and robust payload capacity. The system requirements, detailed in Table 3.1, span four distinct categories: geometric constraints, kinematic capabilities, statics and loading, and pneumatic parameters.

The geometric constraint of a maximum 2.54 cm diameter ensures that the vine robot can exploit gaps significantly smaller than traditional rigid end-effectors [3]. The total assembly footprint restriction ensures that the deployment base does not become a physical obstruction. Kinematically, the maximum local curvature target of $\geq 4.00°/\text{cm}$ is critical for robust steering capabilities. The superposition of the pre-formed discrete bends and the active pouch motor contraction must generate a combined bend of $\geq 180°$ to successfully form a closed-loop topology.

The payload capacity target (≥ 4.50 kg) is designed to establish the viability of the topological transformation. While material yield strength could theoretically support far greater loads, practical mechanical failure typically occurs at the clamping interface due to frictional slipping [2]. Therefore, achieving this target confirms the efficacy of the mechanical anchoring system. The mass constraint (≤ 2.3 kg) directly supports integration onto commercial collaborative robots. Finally, strict regulation of the pneumatic parameters is required to prevent material yield. Operating the main body eversion at ≤ 55 kPa limits hoop and axial stress, while restricting the pouch motor actuation to ≤ 41 kPa mitigates the risk of failure at the thermal impulse welds [4].

Table 3.1: System requirements outlining geometric constraints, kinematic capabilities, loading limits, and operational pressures.

Category	**Parameter**	**Target Specification**	**Justification**
Geometric	Vine Robot Diameter	≤ 2.54 cm	Minimizes spatial profile for constrained environments.
	Total Assembly Volume	$\leq 30.0 \times 15.0 \times 15.0$ cm	Limits size of rigid base to prevent collisions.
Kinematic	Max Local Curvature	$\geq 4.00°/\text{cm}$	Enables tight turning radii for obstacle avoidance.
	Loop Closure Angle	$\geq 180°$	Required to route the tip back to the base clamp.
Static	Payload Capacity	≥ 4.5 kg	Proves load-bearing advantage; bounded by friction.
	Total Assembly Mass	≤ 2.3 kg	Ensures end-effector is light enough for cobots.
Pneumatics	Eversion Pressure	≤ 55 kPa	Keeps stresses below yield strength during growth.
	Actuation Pressure	≤ 41 kPa	Prevents failure of pouch motor heat seals.

Chapter 4

Mechanical Design

4.1 Pouch Motor and Vine Design

The mechanical architecture of the active steering appendage utilizes an axial contraction mechanism superimposed onto a passive, pre-formed backbone. As illustrated in Figure 4.1, a linear array of pneumatic pouch motors is affixed axially along the outer surface of the vine robot. When pressurized, the individual rectangular pouches inflate radially, forcing the inner faces of the pouches to contract axially. This localized axial contraction induces a continuous bending moment, steering the tip of the vine robot toward the actuated side [6].

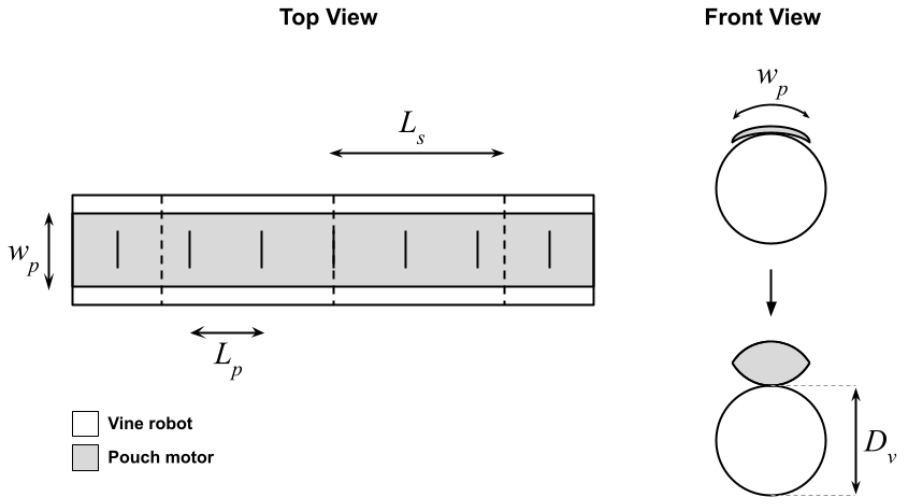

Figure 4.1: Schematic of pouch motor and vine design. L_s describes the length of the segment between pre-form folds. L_p defines the length between the heat seals of the pouch motor, and w_p describes the width of the pouch motor. D_v defines the diameter of the inflated vine robot. The pouch motor is attached to the vine robot with highly adhesive double-sided tape.

Table 4.1: Pouch motor and vine dimensions alongside their respective fabrication materials.

Variable	Description	Nominal Dimension	Component	Material
D_v	Vine Robot Body Diameter	2.54 cm	Vine Robot	LDPE
w_p	Pouch Motor Width	1.27 cm	Pouch Motors	LDPE
L_p	Single Pouch Length	1.27 cm		
L_s	Segment Length	5.08 cm		

The dimensional parameters governing the kinematics of this design are described in Table 4.1. The dimensions of the pouch motor ($w_p = 1.27$ cm, $L_p = 1.27$ cm) are chosen to balance adequate contraction forces with minimal material volume, ensuring that the pouch motor profile does not interfere with inversion and eversion. The axial segment length ($L_s = 5.08$ cm) between pre-form folds is chosen to yield the preferred total bending angle for loop closure. The selection of Low-Density Polyethylene (LDPE) is driven by its exceptional tensile strength-to-weight ratio, high degree of bending compliance, and inherent compatibility with rapid thermal impulse sealing [4].

4.2 Base and Hardware Design

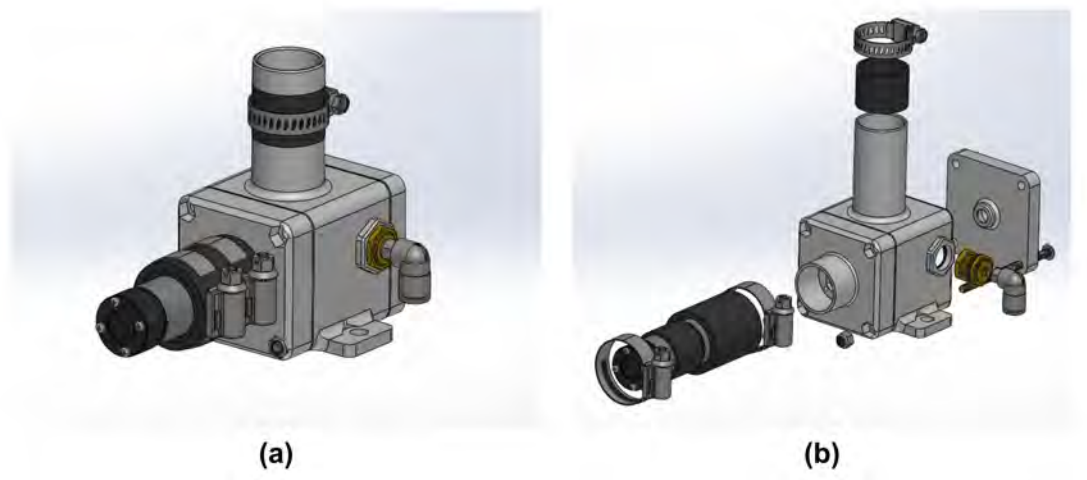

Figure 4.2: Computer-Aided Design (CAD) rendering for a single base illustrating the mechanism utilized to control the eversion and inversion of the vine robot. Image (b) shows an exploded view of the assembly.

The precise control of the eversion and inversion processes is governed by a rigid, 3D-printed base assembly. Building upon the designs from Barhydt et al. [1], Figure 4.2 presents the CAD rendering of a single base, which acts as a sealed pressure vessel that forces the inverted LDPE membrane to evert at the tip when pulling fresh material from an internal spool. Inside the rigid base, a DC motor interfaces directly with the internal tail of the vine robot. By applying torque against the pneumatic eversion pressure, the DC motor regulates

the speed of growth and maintains axial tension. Conversely, applying high torque while simultaneously depressurizing the main chamber enables the active retraction of the vine robot, allowing the grasped payload to be released.

To facilitate complex, multi-point grasping, the system aggregates multiple individual bases into a consolidated end-effector. As seen in Figure 4.3, the full gripper mechanism integrates three independent vine robot appendages alongside a double-clamp assembly driven by linear actuators [1]. Once the actively articulated tips intersect the designated clamping plane, the linear actuators compress the vine robots against a rigid backstop, securely anchoring them and completing the topological loop closure.

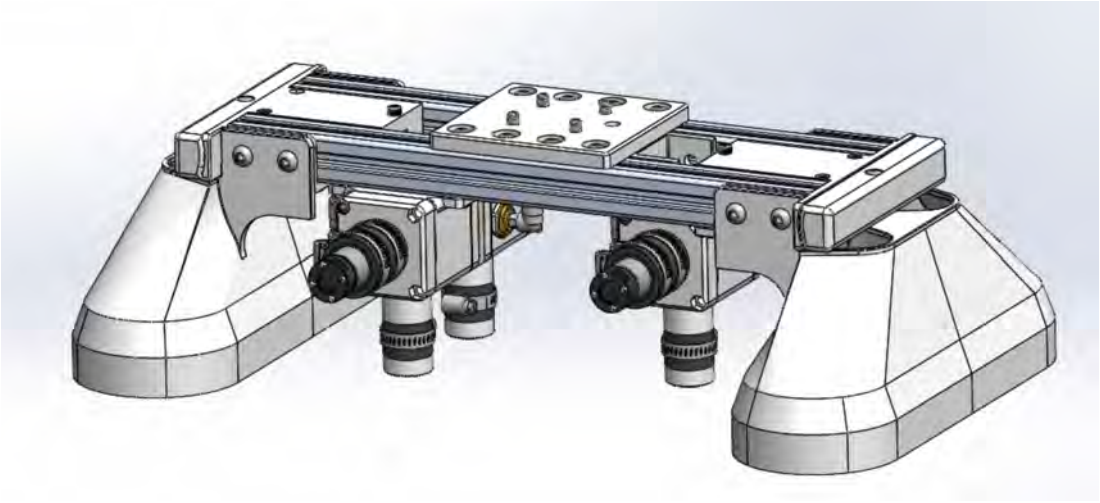

Figure 4.3: CAD Rendering for the full vine robot-clamp gripper mechanism. The system integrates a triple-base configuration to house and control multiple appendages, alongside a double-clamp assembly to securely anchor the tips upon complete loop closure.

4.3 System Architecture and Control Schematic

The system architecture and control schematic for the gripper mechanism, detailed in Figure 4.4, are designed to allow complete teleoperation of all individual system components. A centralized main control unit (MCU) dictates voltage delivery to the DC motors and linear actuators. The primary pneumatic regulator governs the pressure to drive steady eversion, while an array of valves manipulates the pressure delivered to the pouch motor arrays to control the dynamic curvature.

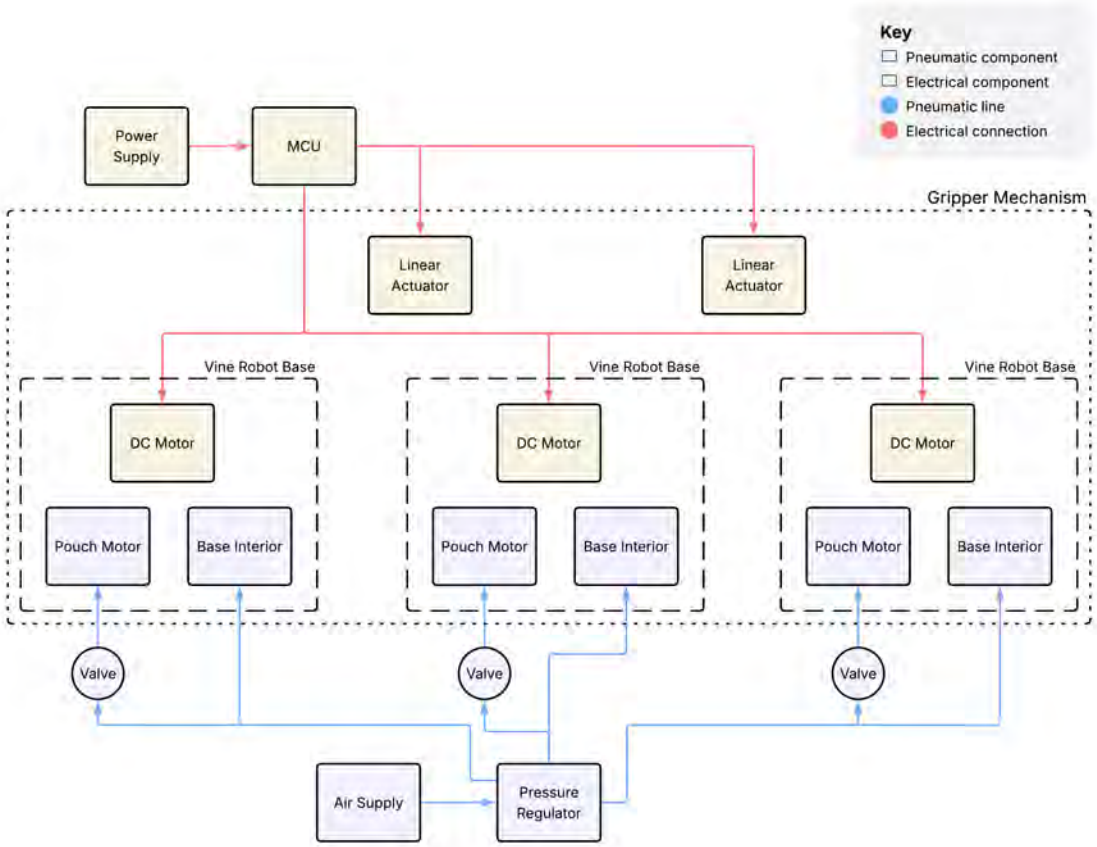

Figure 4.4: System architecture and control schematic for gripper mechanism. The diagram illustrates the routing of the pneumatic supply, highlighting the control between the primary vine robot and the pouch motor array. Pneumatic regulators and valves mediate the airflow, while the motors for the vibe robot bases and the linear actuator for the clamps are controlled with voltages from the MCU.

4.4 Kinematic Modeling: Constant Curvature and Discrete Bends

The spatial trajectory of the articulated vine robot relies on mathematically combining the continuous active curvature of the pouch motors with the discrete pre-programmed bends of the vine robot backbone. For the active continuous curvature, we adopt the mathematical framework demonstrated by Kübler et al. [6]. When a pouch motor of uninflated length L_0 and width w_p is inflated to a pressure P_{pm}, the actuator force F_{pm} is related to the deformation state θ by:

$$F_{pm} = 2L_0 w_p P_{pm} \frac{\cos(\theta)}{\theta} \tag{4.1}$$

The resulting contracted length L_1 is modeled as:

$$L_1 = L_0 \frac{\sin(\theta)}{\theta} \tag{4.2}$$

As the pouch motor inflates, its axis of contraction moves away from the vine robot surface by an offset distance h:

$$h = \frac{L_1}{2} \tan\left(\frac{\theta}{2}\right) \tag{4.3}$$

Assuming force equilibrium where the axial force of the vine robot F_{vine} resists the contraction, the resulting bending angle q per pouch is defined by the equilibrium equation:

$$F_{\text{vine}} \sin(q) = F_{pm} \sin\left(\frac{q}{2}\right) \tag{4.4}$$

The geometric relationship connecting the lengths to the bending angle q and the vine robot diameter D_{vine} is [6]:

$$L_0 = \frac{qL_1}{2\tan\left(\frac{q}{2}\right)} + q(D_{\text{vine}} + h) \tag{4.5}$$

For the passive discrete bends, we utilize the cylindrical representation model defined by Agharese et al. [4]. At each pre-formed fold with a desired joint angle θ_i, the axial distance $\tilde{s}_i$ between the two pinched points on the vine radius is:

$$\tilde{s}_i = 2r\theta_i \tag{4.6}$$

By mathematically superimposing the continuous curvature generated by the active pouch motors over the discrete pre-programmed bends, we can explicitly define the complete spatial trajectory. The continuous curvature κ from the pouch array is defined as:

$$\kappa = \frac{q}{L_0} \tag{4.7}$$

To determine the final position of the actively steered vine robot, the two-dimensional Cartesian coordinates (x_{seg}, y_{seg}) along the localized length h of each segment j are calculated using piecewise constant curvature kinematics. If the continuous curvature is active ($\kappa > 0$), the segment coordinates are:

$$x_{seg}(h) = \frac{1}{\kappa}(\sin(\Phi_{prev} + \kappa h) - \sin(\Phi_{prev})) \tag{4.8}$$

$$y_{seg}(h) = \frac{1}{\kappa}(-\cos(\Phi_{prev} + \kappa h) + \cos(\Phi_{prev})) \tag{4.9}$$

These local segment coordinates are sequentially appended to map the full global displacement (X, Y). At the end of each segment length L_j, the global heading angle Φ_{prev} is updated with the active curvature over that segment and the static pre-formed joint angle θ_j (where applicable) to prepare for the subsequent segment:

$$\Phi_{next} = \Phi_{prev} + \kappa L_j + \theta_j \tag{4.10}$$

As depicted in Figure 4.5, this theoretical kinematic superposition vectors the tip, demonstrating that the displacement curves shift progressively inward toward the base mechanism as the actuation pressure increases from 0 to 41 kPa.

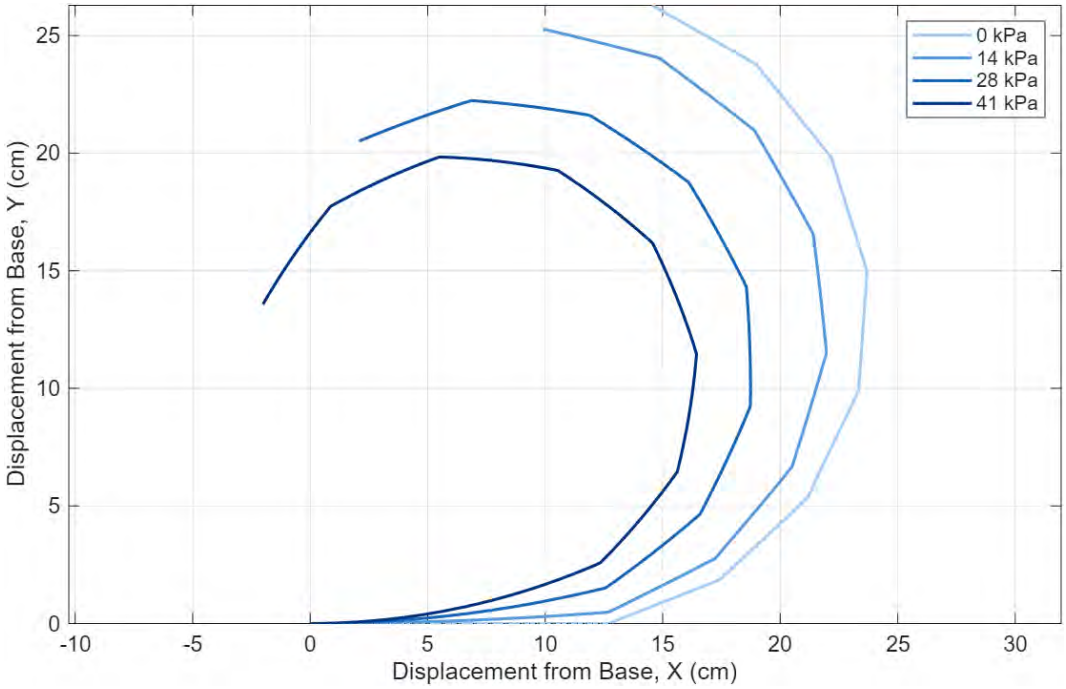

Figure 4.5: Theoretical kinematic displacement of the preformed vine robot under varying actuation pressures. The model maps the bending trajectory by superimposing the continuous curvature generated by the pouch motors onto the discrete preformed structural bends. Discrete bends of $\tilde{s}_i = 0.95$ cm are applied every 5.08 cm, with a 12.7 cm segment at the base. The curves map the actuator pressure increasing from 0 to 41 kPa.

Chapter 5

Fabrication

5.1 Pouch Motor and Vine Robot Fabrication

The fabrication of the active pneumatic manipulator relies on thermal impulse welding and adhesive bonding. The appendages are comprised of two separate LDPE tubes. The primary pressure vessel is formed from a continuous extruded tube of 75-micron-thick LDPE [4]. As outlined in the fabrication process in Figure 5.1, discrete structural folds are mechanically programmed into the membrane prior to deployment. At regular axial intervals of $L_s = 5.08$ cm, 0.95 cm sections ($\tilde{s}_i$) of the LDPE membrane are pinched together and secured using high-strength adhesive tape [4]. These mechanical pinches permanently alter the resting geometry of the inflated cylinder, dictating the baseline curve.

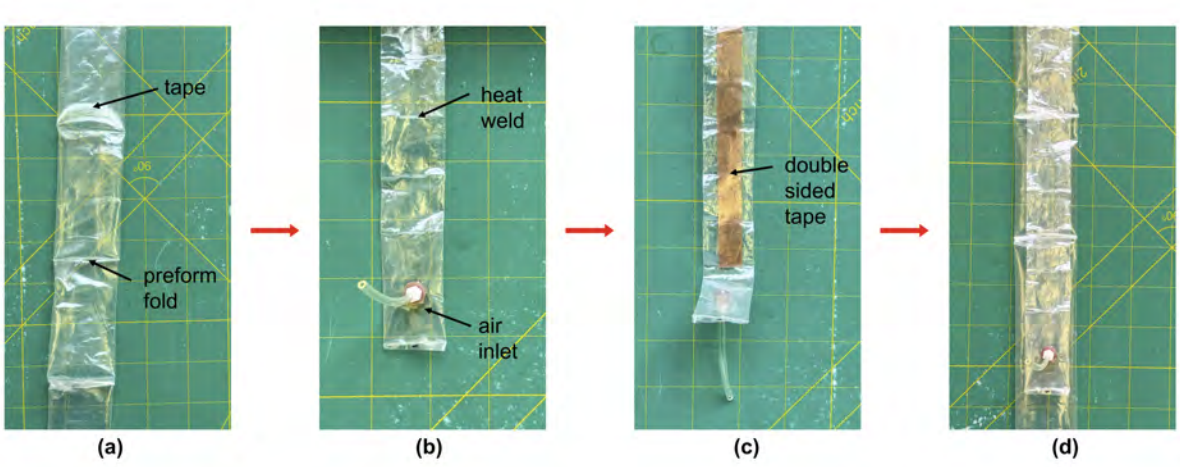

Figure 5.1: Fabrication process of the vine robot and pouch motor assembly. (a) Tape is used to maintain the folded material. Each structural pre-fold pinches 0.95 cm of the primary backbone material, with the folds spaced 5.08 cm apart to define the axial segment. (b) Direct thermal welding is utilized to bond the pouch motor layers together. (c) Highly adhesive double-sided tape is used to mount the pouch motor to the vine robot.

The pouch motors are manufactured independently from the primary vine robot to prevent complex three-dimensional welding [4]. A tube of LDPE is laid flat, and a direct thermal

impulse sealer creates airtight transverse welds at 1.27 cm intervals. Once the array is sealed, it is bonded axially to the outer radius of the pre-formed vine robot using flexible double-sided transfer tape. This sequential fabrication method eases manufacturing and isolates the stresses of the pouch motor and the primary structural vine robot, minimizing failure risks.

5.2 Base and Hardware Integration

Figure 5.2: Fabricated single-base assembly for the pneumatic manipulator. The annotated diagram highlights the critical hardware integration points, including the pressure inlets for the chamber and the DC motor that guides the vine robot material. This rigid interface ensures no pressure is lost during the deployment of the robot into the workspace.

Figure 5.2 displays a fabricated single-base assembly. The rigid deployment bases are 3D-printed, utilizing robust thermoplastic polymers to withstand internal chamber pressures without deformation. The base features elastomer gasket seals, ensuring a zero-loss pneumatic interface where the vine robot attaches to the output nozzle.

A fully integrated closed-loop gripper mechanism prototype, annotated in Figure 5.3, is securely bolted to the end-effector of a Universal Robots UR10 collaborative robotic arm. A critical mechanical addition to the hardware is the implementation of passive funnel guides mounted immediately adjacent to the linear actuator clamps. While the active steering corrects the gross trajectory of the tip, minor deflections can cause the tip to miss the narrow aperture of the clamp. The passive funnels provide a physical mechanical boundary that

captures the advancing tip and mechanically funnels it directly into the clamp of the linear actuator. Since the actuators allow for correction in the plane of bending, the funnel is specifically designed to compensate for errors in out-of-plane bending, while minimizing coverage in-plane.

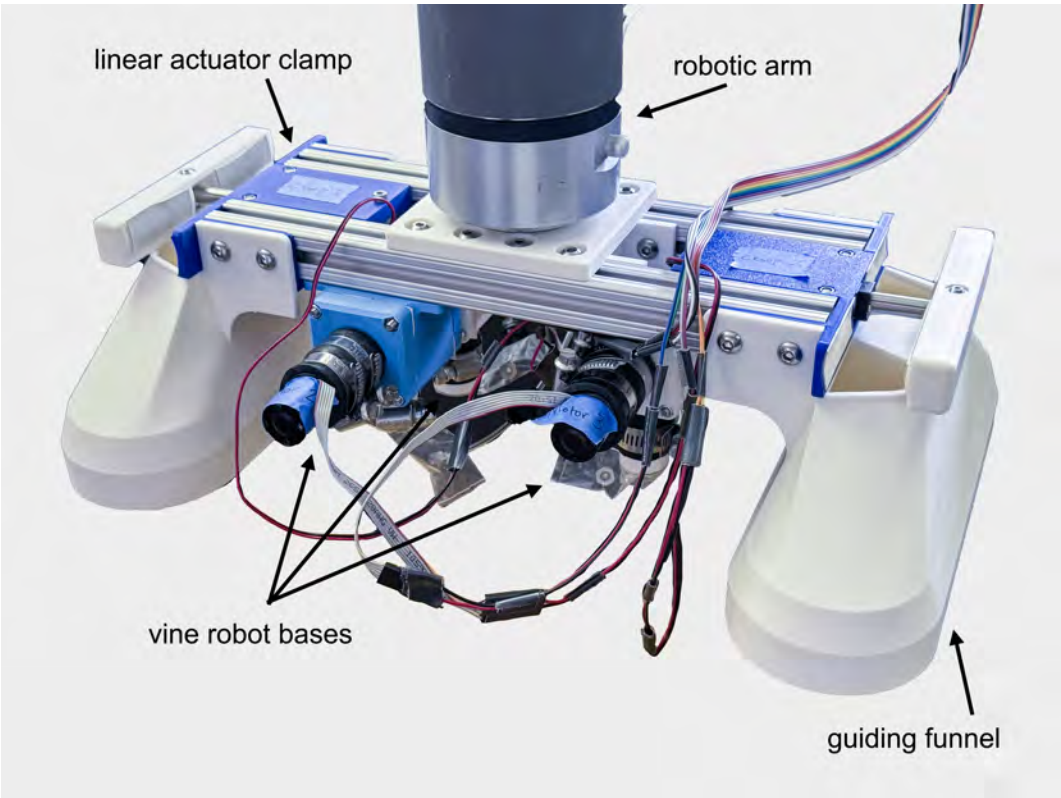

Figure 5.3: Annotated physical prototype of the fully integrated closed-loop gripper mechanism. The structure is mounted to a UR10 robotic arm for positioning. The assembly features three independent deployment bases to actuate the vine robots, alongside passive funnel guides that physically direct the growing tips into two anchoring clamps. This configuration secures the topological loop required for manipulation.

Chapter 6

Experimentation

The experimental phase is designed to evaluate the kinematic behavior of the integrated pouch motors, map the displacement curves, and validate the maximum payload capacities. As shown in the experimental setup in Figure 6.1, the vine robot is deployed in an unconstrained environment with a camera fixed perpendicular to effectively eliminate distortion [6].

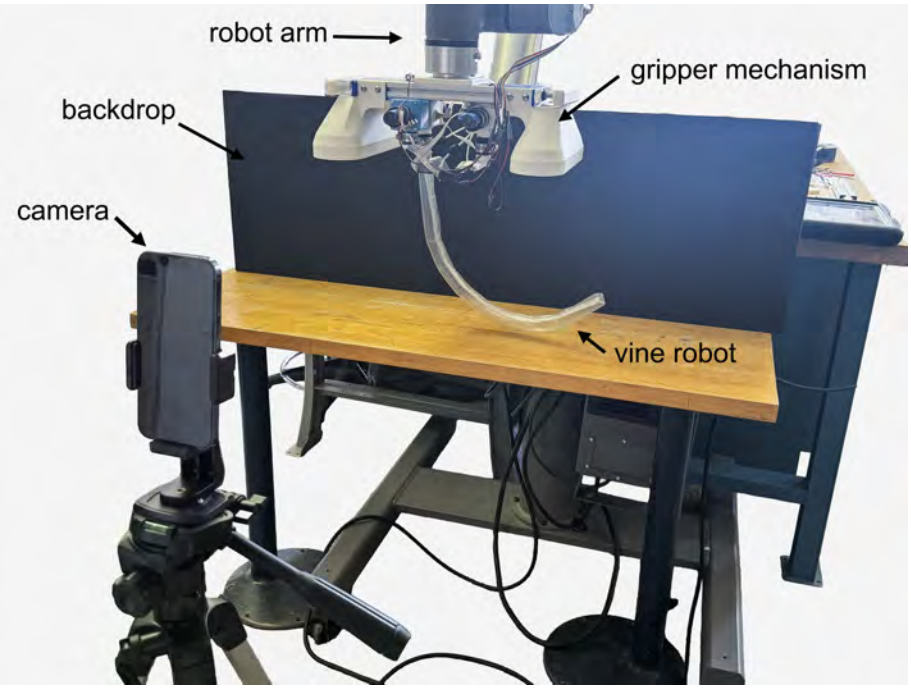

Figure 6.1: Experimental setup for kinematic characterization and system demonstration. A camera is mounted perpendicularly to the gripper's workspace. This controlled environment was utilized both to record the dynamic loop-closure sequence and to capture the bending trajectories required for the curvature analysis.

To capture the bending profiles, the main eversion chamber is pressurized to an eversion pressure, and the DC motor is actuated, extending the robot until the pouch motor array is fully everted. The pneumatic line feeding the pouch motor array is then incrementally pressurized via the regulator and valve from 0 kPa to a maximum of 44 kPa in discrete steps.

At each pressure interval, sequential photographs of the actuated manipulator are captured. Figure 6.2 outlines the image analysis process used to isolate the physical bending profile by utilizing Fiji (ImageJ) software. The spatial coordinates of the vine robot's central axis are isolated, yielding empirical coordinates, which are then plotted against the theoretical predictions to quantify the baseline accuracy of the mathematical framework.

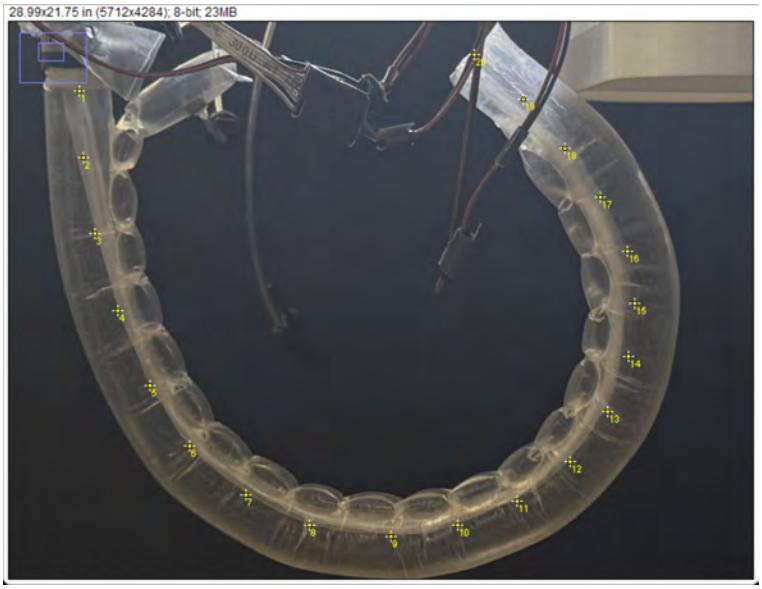

Figure 6.2: Screenshot of the image analysis process for kinematic characterization. Sequential photographs of the actuated manipulator were processed using Fiji (ImageJ) software.

To test the system against the static requirements, a maximum payload test is conducted. The three independent vine robots are everted, actively steered through the funnel guides via the pouch motors, and securely anchored by the double-clamp linear actuators, finalizing the topological loop closure. The internal eversion pressure is completely vented, allowing the vine robot to transition into a highly compliant tensile strap. Sequential weights are progressively added to the created closed-loop until catastrophic mechanical slip failure is observed at the clamping interface [2].

Chapter 7

Results

7.1 Loop Closure and Steering Demonstration

The primary functional validation is the ability of the active steering appendage to successfully and repeatedly achieve the closed-loop topological state. A sequential time-lapse in Figure 7.1 records the multi-appendage eversion and interlocking process.

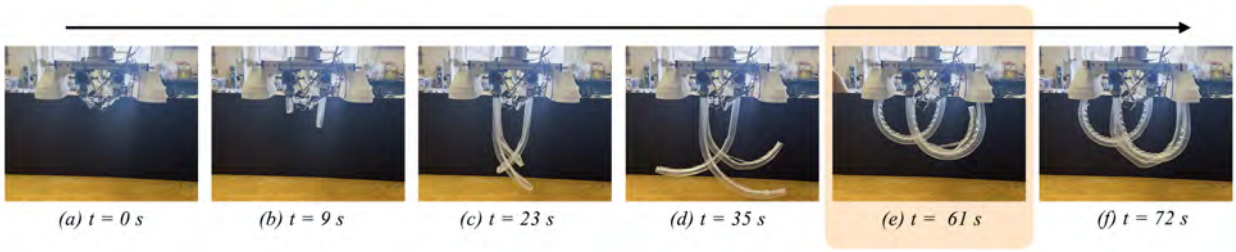

Figure 7.1: Sequential demonstration of the multi-appendage eversion and closed-loop interlocking process. The time-lapse captures the three vine robots everting from their respective deployment bases. Upon reaching the required length, the pouch motor array is pressurized at $t = 61$ s (indicated by the orange highlight), actively steering the tips toward the passive funnel guides. The sequence concludes with the mechanical clamps securing the tips, finalizing the load-bearing closed-loop topology.

During the initial deployment phase (spanning from $t = 0$ s to $t = 35$ s), the three vine robots grow outward, relying strictly on their passive pre-formed bends. At $t = 61$ s, the active steering is engaged, and the pouch motors are pressurized. The immediate axial contraction sharply increases local curvature, actively pivoting the tips toward the passive funnel guides. By $t = 72$ s, the tips are fully seated within the guides, and the linear actuators compress, successfully locking the topology. This demonstration validates that active steering successfully corrects the passive trajectory gap.

7.2 Payload Grasping

As demonstrated in Figure 7.2, the system was subjected to grasping tasks to confirm the stability, compliance, and versatility of the grasp. In the first test, a singular vine robot appendage securely enclosed a rigid cylindrical object (mug). This infinite bending compliance prevented the application of any concentrated point loads that could shatter the mug or cause the end-effector to slip [1]. In the second test, the system tackled a heavy, asymmetric bundle of irregular aluminum extrusions with two of the vine robots. Once lifted, the high tensile strength of the deflated LDPE tightly cinched the loose aluminum profiles together, stabilizing the uneven mass distribution during dynamic transport.

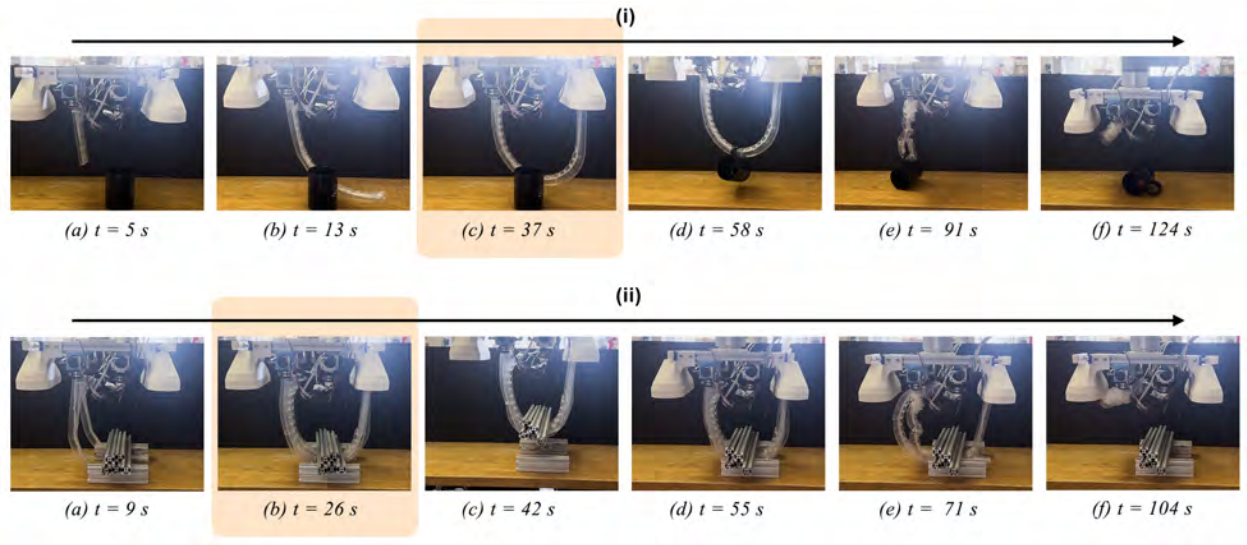

Figure 7.2: Experimental demonstration of closed-loop payload manipulation. The multi-appendage system is shown successfully interlocking, lifting, and placing target objects of varying geometries and mass. In sequence (i), the manipulator secures and transports a rigid cylindrical object (mug) with a single vine robot appendage. In sequence (ii), the system demonstrates its high-capacity load-bearing and conformal capabilities by lifting a heavier, irregular payload (a bundle of aluminum extrusions) with two vine robot appendages. The moment at which the pouch motors are actuated is highlighted in orange.

7.3 Kinematic Characterization

To precisely quantify the effect of the pouch motors on the system's geometry, the bending per unit length was analyzed over the full operational pressure range. As plotted in Figure 7.3, the empirical data demonstrates a strong non-linear correlation between the pouch motor pressure and the resulting curvature. A quadratic polynomial curve fit maps the relationship:

$$y = -0.00036x^2 + 0.05113x + 3.252 \tag{7.1}$$

where x represents the actuation pressure in kPa, and y represents the curvature in $^\circ$/cm [6].

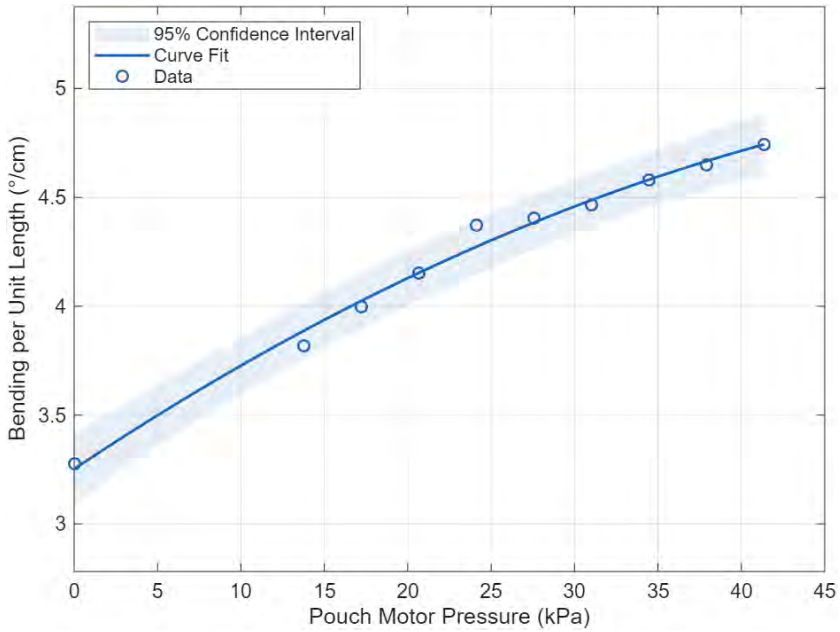

Figure 7.3: Experimental characterization of the manipulator's bending per unit length as a function of actuation pressure. The empirical data demonstrate a strong non-linear correlation between the pouch motor pressure and the resulting curvature. A quadratic polynomial curve fit ($y = -0.00036x^2 + 0.05113x + 3.252$) is overlaid on the data points. The 95% confidence interval is overlaid on the curve.

The data indicate a baseline passive bending of approximately 3.28°/cm at 0 kPa. As pressure increases, the active bending per unit length increases quadratically, reaching an empirical maximum of 4.74°/cm at the 44 kPa threshold. The negative leading coefficient (-0.00036) reveals diminishing returns at higher actuation pressures as the pouch motor expands radially to its volumetric limit. Nonetheless, the maximum recorded curvature comfortably exceeds the 4.00°/cm target requirement.

7.4 Model Validation

The theoretical kinematic superposition model was verified against the extracted physical coordinates from the image analysis. As shown in Figure 7.4, the theoretical kinematic superposition model reliably predicts the two-dimensional bending trajectories of the vine robot at discrete pouch motor pressures ranging from 0 to 41 kPa.

To rigorously evaluate the spatial accuracy of the model, a minimum Euclidean distance root mean square error (RMSE) analysis was conducted across the operational pressure spectrum. The results of this analysis, along with the maximum local errors, are detailed in Table 7.1.

The analysis demonstrates that the kinematic model maintains a high degree of fidelity at the boundaries of the actuation range (0 kPa and 41 kPa), yielding an RMSE of 0.7348 cm and 0.5451 cm, respectively. The maximum local error and RMSE peak at intermediate actuation pressures (e.g., 14 kPa), reaching a maximum RMSE of 2.0927 cm. These quantitative

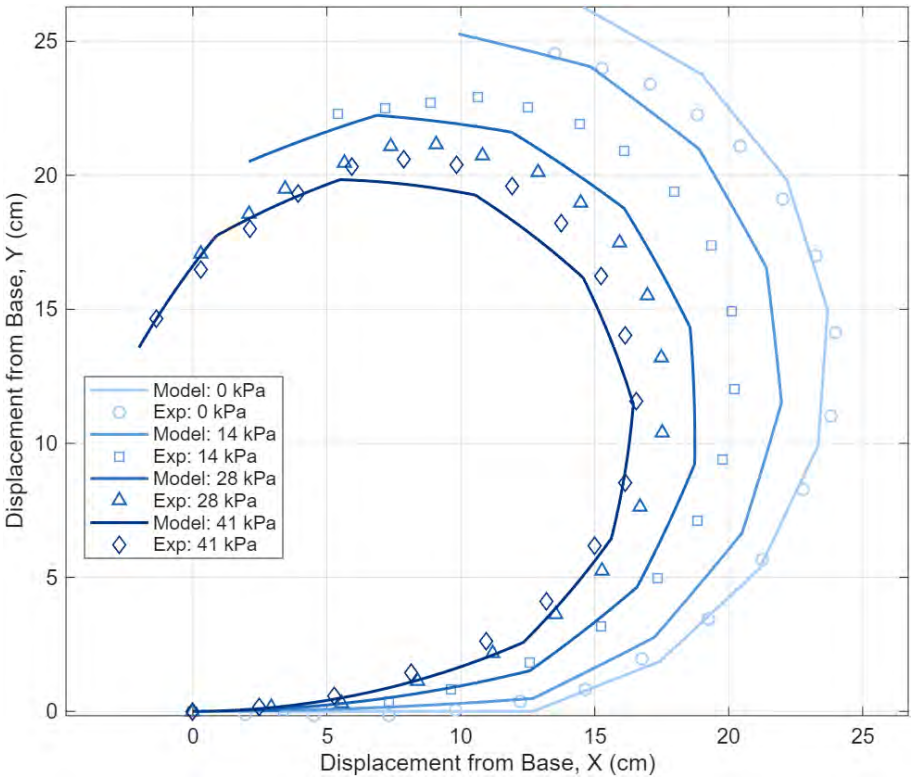

Figure 7.4: Comparison of the theoretical kinematic superposition model against empirical displacement data. The solid lines represent the predicted bending trajectories of the vine robot at discrete pouch motor pressures ranging from 0 to 41 kPa. The superimposed markers denote the actual physical coordinates extracted during experimental validation.

deviations from the theoretical model can be attributed to out-of-plane torsional twisting of the vine robot as well as complex buckling behaviors that the purely 2D planar, constant-curvature assumption of the mathematical framework does not capture.

Table 7.1: Error analysis comparing theoretical kinematic predictions to empirical displacement data.

Actuation Pressure (kPa)	**Root Mean Square Error (cm)**	**Maximum Error (cm)**
0	0.7348	2.0378
14	2.0927	5.3999
28	1.3226	3.8793
41	0.5451	1.0423

7.5 System Performance Assessment

Table 7.2 summarizes the actual measured values derived from the experimental testing against the initial target specifications. The integrated active steering loop closure system demonstrated overwhelming success in its kinematic and kinetic goals. The maximum local curvature (4.74°/cm) and the loop closure angle capabilities (229.4°) exceeded the required baselines. Furthermore, the payload capacity reached 6.3 kg with an assembly mass of only 1.4 kg, yielding a payload-to-weight ratio of approximately 4.5. These results support the fundamental strength advantages of transitioning from an open-loop flexural system to a closed-loop tensile system.

Table 7.2: Comparison of target system specifications and experimental values.

Category	**Parameter**	**Measured Value**	**Status**	**Target**
Geometric	Vine Robot Diameter	2.54 cm	Achieved	≤ 2.54 cm
	Total Assembly Volume	$35.6 \times 20.0 \times 26.7$ cm	Not Met	$\leq 30.0 \times 15.0 \times 15.0$ cm
Kinematic	Max Local Curvature	4.74°/cm	Exceeded	≥ 4.00°/cm
	Loop Closure Angle	229.4°	Exceeded	≥ 180°
Static	Payload Capacity	6.3 kg	Exceeded	≥ 4.5 kg
	Total Assembly Mass	1.4 kg	Exceeded	≤ 2.3 kg
Pneumatics	Eversion Pressure	62 kPa	Not Met	≤ 55 kPa
	Actuation Pressure	41 kPa (Max)	Achieved	≤ 41 kPa

Two specifications, however, were not met. First, the total assembly footprint exceeded the target boundaries to accommodate the triple-base configuration alongside the volume of the passive guide funnels. Second, the eversion pressure observed at 62 kPa exceeded the strict 55 kPa maximum safety threshold. This need for higher eversion pressure could be due to the internal tail friction generated by the additional material from the pouch motors or small manufacturing discrepancies.

Chapter 8

Conclusion

8.1 Summary

This research successfully designed, fabricated, and validated an active steering articulation system integrated with small-scale soft growing robots to guarantee reliable loop closure grasping. By fabricating low-profile pneumatic pouch motors from LDPE and integrating them onto mechanically pre-formed vine robot backbones, the system achieved a highly effective hybrid steering model. The experimental validation confirmed that the superimposed active curvature corrects passive trajectory deviations, consistently guiding the tip into passive guiding funnels and anchoring clamps. Upon deflation, the resulting topological transition to a closed loop facilitated the manipulation of complex geometries, lifting payloads up to 6.3 kg while maintaining a compliant, non-damaging contact interface. The resulting system represents a highly capable, lightweight solution tailored for handling heavy yet fragile objects in constrained, unpredictable environments.

8.2 Limitations and Future Work

Despite its successes in payload handling and kinematic articulation, the current iteration of the system exhibits notable limitations that dictate the trajectory of future work. The failure to meet the eversion pressure constraints, requiring 62 kPa rather than the targeted 55 kPa, poses long-term cyclic fatigue risks to the LDPE material. Future iterations could explore integrating the active steering chambers directly into the primary pressure vessel via welding, similar to integrated cPAM architectures [6]. This integration would eliminate stiffening adhesive layers. Moreover, simply increasing the diameter of the vine robot could relieve material volume and friction constraints. Additionally, the reliance on a passive funnel to physically capture the tip increases system footprint and indicates that the 2D planar active steering provided by a single pouch motor array is insufficient for highly perturbed 3D environments. Future designs should incorporate dual pouch motor arrays, enabling a 3D workspace to actively compensate for out-of-plane bending. Finally, high-friction material, such as Dycem [1], should be incorporated at the clamping interface to optimize the maximum payload toward the ultimate tensile limits of the LDPE.

References

[1] K. Barhydt, O. G. Osele, S. Kodali, C. du Pasquier, C. M. Hartquist, H. H. Asada, and A. M. Okamura. "Loop closure grasping: Topological transformations enable strong, gentle, and versatile grasps." *Science Advances*, **11**(50), Dec. 2025, eady9581. DOI: 10.1126/sciadv.ady9581.

[2] O. G. Osele, K. Barhydt, N. Cerone, A. M. Okamura, and H. H. Asada. "Tip-Clutching Winch for High Tensile Force Application with Soft Growing Robots." *2024 IEEE International Conference on Robotics and Automation (ICRA)*, May 2024. DOI: 10.1109/ICRA57147.2024.10610362.

[3] E. W. Hawkes, L. H. Blumenschein, J. D. Greer, and A. M. Okamura. "A soft robot that navigates its environment through growth." *Science Robotics*, **2**(8), July 2017, eaan3028. DOI: 10.1126/scirobotics.aan3028.

[4] N. Agharese and A. M. Okamura. "Configuration and Fabrication of Preformed Vine Robots." *arXiv*, June 2023. DOI: 10.48550/arXiv.2306.01166.

[5] L. H. Blumenschein, M. M. Coad, D. A. Haggerty, A. M. Okamura, and E. W. Hawkes. "Design, Modeling, Control, and Application of Everting Vine Robots." *Frontiers in Robotics and AI*, **7**, Nov. 2020, p. 548266. DOI: 10.3389/frobt.2020.548266.

[6] A. M. Kübler, C. du Pasquier, A. Low, B. Djambazi, N. Aymon, J. Förster, N. Agharese, R. Siegwart, and A. M. Okamura. "A Comparison of Pneumatic Actuators for Soft Growing Vine Robots." *Soft Robotics*, **11**(5), 2024. DOI: 10.1089/soro.2023.0169.

[7] C. du Pasquier, S. Jeong, and A. M. Okamura. "Finite Element Modeling of Pneumatic Bending Actuators for Inflated-Beam Robots." *IEEE Robotics and Automation Letters*, **8**(11), Nov. 2023, pp. 7416–7423.

[8] K. Becker, C. Teeple, N. Charles, Y. Jung, D. Baum, J. C. Weaver, L. Mahadevan, and R. Wood. "Active entanglement enables stochastic, topological grasping." *Proceedings of the National Academy of Sciences (PNAS)*, Sept. 2022. DOI: 10.1073/pnas.2209819119.

[9] G. Kang, Y.-J. Kim, S.-J. Lee, S. K. Kim, D.-Y. Lee, and K. Song. "Grasping through dynamic weaving with entangled closed loops." *Nature Communications*, **14**, Aug. 2023, p. 4633. DOI: 10.1038/s41467-023-40358-y.